

ATTACHMENT 4

STRUCTURAL INTEGRITY ASSOCIATES, INC

**FLAW EVALUATION OF INDICATIONS IN THE
NINE MILE POINT UNIT 2 STEAM DRYER VERTICAL SUPPORT
PLATES CONSIDERING EXTENDED POWER UPRATE
FLOW INDUCED VIBRATION LOADING**

(NON-PROPRIETARY)

Information in this Attachment is proprietary.

Report No. 1000814.401
Revision 0
Project No. 1000814
July 2010

**Flaw Evaluation of Indications in the Nine Mile Point Unit 2
Steam Dryer Vertical Support Plates
Considering Extended Power Uprate
Flow Induced Vibration Loading**

Prepared for:

Constellation Energy Nuclear Group
Oswego, NY
Purchase Order No. 7719780, Rev. 0

Prepared by:

Structural Integrity Associates, Inc.

Prepared by:  
Date: 7/28/10
Y. Chen, P. Eng., Ph. D.
D. Sommerville, P.E.

Reviewed by:  
Date: 7/28/10
S. Tang
J. Wu

Approved by: 
Date: 7/28/10
D. Sommerville, P.E.

REVISION CONTROL SHEET

Document Number: 1000814.401

Title: **Flaw Evaluation of Indications in the Nine Mile Point Unit 2 Steam Dryer
Vertical Support Plates Considering Extended Power Uprate Flow Induced
Vibration Loading**

Client: Constellation Energy Nuclear Group

SI Project Number: 1000814

Quality Program: Nuclear Commercial

Section	Pages	Revision	Date	Comments
1	1-1	0	7/28/10	Initial Issue
2	2-1			
3	3-1 – 3-6			
4	4-1- 4-2			
5	5-1 – 5-7			
6	6-1 – 6-21			
7	7-1			
8	8-1			
A	A-1 – A-2			

Table of Contents

<u>Section</u>	<u>Page</u>
1.0 OBJECTIVE	1-1
2.0 BACKGROUND	2-1
3.0 METHODOLOGY	3-1
3.1 General Methods.....	3-1
3.2 CLTP Flaw Evaluation Methodology.....	3-2
3.3 EPU Flaw Evaluation Methodology.....	3-5
4.0 ASSUMPTIONS.....	4-1
5.0 INPUT DATA.....	5-1
5.1 Vertical Support Plate Geometry	5-1
5.2 Indication Location and Orientation	5-2
5.3 CLTP FIV Loads and Boundary Conditions	5-3
5.4 Sample Stress Time History.....	5-3
6.0 ANALYSIS	6-1
6.1 Finite Element Model	6-1
6.1.1 <i>Un-cracked Model</i>	6-1
6.1.2 <i>Cracked Models</i>	6-1
6.1.3 <i>Boundary Conditions</i>	6-2
6.2 Uncracked Stress Distributions.....	6-3
6.3 Finite Element Fracture Mechanics Analysis Results	6-3
6.4 Stress Time History Evaluation	6-5
6.5 CLTP FIV Fracture Mechanics Evaluation	6-6
6.6 EPU FIV Fracture Mechanics Evaluation.....	6-7
7.0 CONCLUSIONS	7-1
8.0 REFERENCES.....	8-1
APPENDIX A INPUT FILE LISTING	A-1

List of Tables

<u>Table</u>	<u>Page</u>
Table 5-1. Forces and Moments applied on the surfaces.....	5-7
Table 6-1. Stress Intensity Histogram for 120 Second Stress Time History - CLTP.....	6-19
Table 6-2. Stress Intensity Range Histogram for 120 Second Stress Time History - CLTP.....	6-20

List of Figures

<u>Figure</u>	<u>Page</u>
Figure 3-1. Fatigue Threshold Stress Intensity Factor Data [8].....	3-6
Figure 5-1. Schematic Identifying the Location of all Indications in the NMP2 Steam Dryer Vertical Support Plates.	5-3
Figure 5-2. Schematic of the Inner and Outer Bank Vertical Support Plate Weld Configurations.....	5-4
Figure 5-3. Representative Photographs of the NMP2 Vertical Support Plate Indications.....	5-4
Figure 5-4. Boundary Conditions for the 3-D sub model provided by CDI.....	5-5
Figure 5-5. Forces (a) and moments (b) Applied on the surfaces of the 3-D sub model.....	5-6
Figure 6-1. Illustration of Double-sided welds between Support and Spacer Plates, outer hood.	6-9
Figure 6-2. Finite Element Model for Uncracked Support Plate Assembly.....	6-10
Figure 6-3. Finite Element Model with 0.5” long Double-sided Cracks.....	6-10
Figure 6-4. Finite Element Model with 1.0” long Double-sided Cracks.....	6-11
Figure 6-5. Finite Element Model with 1.5” long Double-sided Cracks.....	6-11
Figure 6-6. Finite Element Model with 2.0” long Double-sided Cracks.....	6-12
Figure 6-7. Finite Element Model with 2.5” long Double-sided Cracks.....	6-12
Figure 6-8. Finite Element Model with 3.0” long Double-sided Cracks.....	6-13
Figure 6-9. Boundary Conditions for the Force FEM.....	6-13
Figure 6-10. Boundary Conditions for the Displacement FEM.....	6-14
Figure 6-11. Stress Intensity Contours from the Force FEM.....	6-14
(Note: Units are in psi).....	6-14
Figure 6-12. Stress Intensity Contours from the Displacement FEM.....	6-15
(Note: Units are in psi).....	6-15
Figure 6-13. K_{IEQ} Distribution along crack front for 2.0 inch Crack Case.....	6-15
Figure 6-14. Refined Finite Element Model with 2.0” long Double-sided Cracks.	6-16
Figure 6-15. ΔK_{IEQ} Distribution across Left Side Crack Front for Various Crack Depths - CLTP.....	6-16

Figure 6-16. ΔK_{IEQ} Distribution across Left Side Crack Front for Various Crack Depths - EPU.....	6-17
Figure 6-17. Mean ΔK_{IEQ} for Bounding Crack Side (Left Side) for Various Crack Depths.....	6-17
Figure 6-18. Mean ΔK_{IEQ} for Bounding Crack Side (Left Side) for Various Crack Depths, CLTP, Load and Displacement Controlled.....	6-18
Figure 6-19. 120 Second Stress Time History from Peak Stress Location in Vertical Support [4] Plate – Shell Model, CLTP.....	6-18
Figure 6-20. Stress Histogram for 120 Second Stress Time History.....	6-19
Figure 6-21. Stress Range Histogram for 120 Second Stress Time History.....	6-20
Figure 6-22. Fatigue Crack Growth Calculation for Bounding Vertical Support Plate Indication - CLTP.	6-21

1.0 OBJECTIVE

Indications were identified in the Nine Mile Point Unit 2 (NMP2) steam dryer vertical support plates during the April 2010 refueling outage steam dryer visual examinations [1]. The 2010 examinations were the first to be performed of the internal surfaces of the NMP2 steam dryer. This report documents a flaw evaluation of the bounding outer hood vertical support indication in the NMP2 steam dryer considering extended power uprate (EPU) flow induced vibration (FIV) loading. The objectives of this analysis are:

1. Assess whether the current licensed thermal power (CLTP) FIV loads result in growth of a crack to the dimensions observed during the 2010 IVVI [1]. This is intended to validate both the underlying assumptions and overall crack growth model by comparing predictions with field measurements.
2. Assess whether the outer, middle, and inner hood vertical support indications are expected to experience fatigue crack growth (FCG) from the EPU FIV loading.

2.0 BACKGROUND

Constellation Energy Nuclear Group (CENG) is pursuing an EPU for the NMP2 nuclear power plant. As part of the EPU application process it is necessary to determine if existing indications in the steam dryer assembly are anticipated to experience FCG when the plant is operated at EPU conditions. Consequently, SI has performed flaw evaluations for all previously identified indications in the NMP2 steam dryer [2, 3].

Indications were identified in the NMP2 steam dryer vertical support plates during the April 2010 refueling outage steam dryer visual examinations [1]. Since these cracks had not been identified at the time the previous steam dryer flaw evaluations were performed, this analysis documents the EPU flaw evaluation for the newly identified indications.

This flaw evaluation is performed using geometry and stress input provided by Continuum Dynamics, Inc. (CDI) [4].

3.0 METHODOLOGY

This section describes the methods used to perform the steam dryer vertical support plate flaw evaluation. The general guidance of BWRVIP-139-A [5] is considered in this analysis. The methods used to address objectives 1 and 2 are referred to as the CLTP and EPU flaw evaluation, respectively.

3.1 General Methods

The flaw evaluation is performed using the following methods:

1. The vertical support plate welds contain indications that appear to initiate in and remain within the welds that join the vertical support plates to the hood or intermediate plate. The presence of the indications in the weld material, as well as the lack of branching in the flaws, suggests that the cracks are not caused by intergranular stress corrosion cracking (IGSCC).
2. The range of stress intensity factor used for calculation of fatigue crack growth (FCG), ΔK_I , is calculated using the range of stress contributed by the FIV loading only.
3. Linear Elastic Fracture Mechanics (LEFM) and FCG calculations are performed for a range of flaw sizes chosen such that they bound the indication lengths reported in the Indication Notification Form (INF) [1]. Indication lengths reported in the INF [1] are obtained by scaling the visual record by the weld dimensions given in the design drawings [6a, 6b, 6c].
4. FCG is determined using the methods contained in Article C-3000 of the ASME B&PV Code, Section XI [7]. Based upon the location of the crack in the weld metal, the crack is not believed to be IGSCC; thus, SCC growth is not considered.

5. For small ΔK_I , credit is taken for the threshold stress intensity factor range for FCG provided in Reference [8] for stainless steels, ΔK_{ITH} . Figure 3-1 shows fatigue threshold stress intensity factor data for stainless steel in an air environment [8]. Since the indications considered for this analysis are in the steam dome it is appropriate to use these data.
6. The middle and inner hoods are bounded by {
 }
 } and observed flaw lengths [1]; therefore, this analysis considers only the outer hood configuration, stresses, and flaw lengths.

3.2 CLTP Flaw Evaluation Methodology

The following methodology is utilized for the CLTP flaw evaluation:

1. Construct a three-dimensional (3-D) sub model of the outer hood vertical support plate in the vicinity of the observed cracks.
2. Apply CLTP force and moment boundary conditions, provided by CDI, to the sub model obtained from the 3-D shell element finite element model (FEM) of the NMP2 steam dryer assembly.
3. Obtain equivalent displacement boundary conditions on the boundary surfaces of the 3-D sub model obtained from a static solution of the sub model using the force and moment boundary conditions.
4. Model the vertical support plate cracking using crack tip singularity elements. Multiple cracked cases are considered for this study in order to assess the trend of stress intensity factor with crack depth.
5. Considering that the vertical support plate is subjected to in plane and out of plane loads, the Mode I, Mode II, and Mode III stress intensity factors, K_I , K_{II} , K_{III} , calculated from the finite element fracture mechanics analysis, are converted into an equivalent Mode I stress intensity factor, K_{IEQ} .

6. FCG of the indication is calculated using the methods of Appendix C, Section XI, of the ASME B&PV Code [7] and using the average ΔK_{IEQ} along the crack front. Where the ΔK_{IEQ} is less than a conservatively estimated threshold stress intensity factor for FCG for austenitic stainless steel, ΔK_{ITH} , no FCG is predicted to occur. Although a ΔK_{ITH} is not included in the Appendix C FCG curves for austenitic stainless steel it is supported by test data presented in [8]. The ΔK_{ITH} used for this analysis is the lower bound ΔK_{ITH} for a R-ratio of ~ 0.9 ; this value is extrapolated from the 18-8 austenitic stainless steel test data presented in Figure 3-1 [8].
7. Review stress time history data from the CDI shell model of the steam dryer, at the peak stress location of the vertical support plate corresponding to the longest indication identified in 2010 [1], to develop a histogram of FIV stress ranges.
8. Use the stress range histogram to obtain estimates for the numbers and amplitudes of stress cycles occurring during a block of time.
9. Use the stress range histogram to calculate relative scaling factors between the stress ranges which are subsequently used to scale the stress intensity factors calculated from the finite element fracture mechanics evaluation to represent different stress range categories at CLTP and EPU power levels.
10. Perform a FCG calculation using the histogram stress ranges and scaling factors to predict the time required to grow an incipient crack to the length observed in 2010 [1].

Continuum Dynamics, Inc (CDI) provided SI with a 3-D sub model of the outer hood vertical support plate geometry which contains the outer hood, vertical support plate, cover plate, spacer plate and all the welds in the vicinity of the cracks [4]. SI modified the geometry to model cracks in both fillet welds joining the vertical support plate to the spacer plate in order to perform a finite element fracture mechanics analysis.

CDI provided zero-to-peak (0-peak) CLTP FIV loads on the boundaries of the sub model [4]. Displacement boundary conditions are obtained by solving a static analysis of the sub model using the force and moment boundary conditions provided by CDI. The displacement solution on the sub model boundaries are extracted from the FEM and applied as boundary conditions for subsequent fracture mechanics analysis. This method enables consideration of a displacement controlled load for the fracture mechanics analyses.

The finite element fracture mechanics analysis is performed using the ANSYS finite element analysis software [9]. Cracks are modeled using quadratic elements with the mid side nodes moved to the quarter point location such that the stress singularity at the crack tip is simulated. The crack tip elements are modeled using ANSYS SOLID95 3-D solid elements with quadratic shape functions. The remainder of the model is built using ANSYS SOLID45 3-D solid elements with linear shape functions. Multiple crack cases considering dimensions that are both less than and larger than the bounding observed crack dimension are considered in this evaluation; this enables determination of the trend of stress intensity factor with crack length.

The Mode I, Mode II, and Mode III stress intensity factors, K_I , K_{II} , K_{III} , are calculated at each node along the crack front using the ANSYS KCALC command [9]. The equivalent stress intensity factor, K_{IEQ} , for the plane strain condition is calculated based on the energy release rate theory from Reference [10] as follows:

$$K_{IEQ} = \sqrt{K_I^2 + K_{II}^2 + \frac{K_{III}^2}{1-\nu}} \quad (1)$$

where ν is the Poisson's ratio.

Since mean stresses contributed by loads such as deadweight, static pressure, steady state thermal, fit-up or weld residual stresses are not known, the highest mean stress effect is conservatively considered in this evaluation. Consequently, the mean stresses at the crack location are conservatively assumed to be equal to or larger than the amplitude of the 0-peak FIV loads. This results in the K_{IEQ} being considered as $\Delta K_I/2$, where ΔK_I is the range of stress intensity factor used for calculating FCG and for comparison to the threshold stress intensity factor for FCG, ΔK_{th} .

Stress time history data is evaluated to determine the distribution of stress cycles in a 120 second time segment of the steam dryer FIV stress results provided by CDI [4]. A sample stress time history extracted from the steam dryer shell model at the location of peak stress in the vertical support plate is evaluated and considered representative of the stress cycles experienced by the vertical support plate. Further, the distribution of stress ranges determined from the stress time history are considered representative of the distribution expected for the vertical support plate. The peaks and valleys of the stress time history data are identified and sorted such that the number and range of stress cycles can be identified. A histogram of stress cycles is calculated using the data analysis feature of Microsoft Excel. Finally, cycle counts are determined using conservative stress ranges based upon the histogram bins. These cycle counts are used to calculate the number and range of stress cycles expected during an arbitrary length of time at CLTP conditions. The cycle counts and relative cycle amplitudes are used to calculate FCG at CLTP conditions.

3.3 EPU Flaw Evaluation Methodology

The following methodology is utilized for the EPU flaw evaluation:

1. Calculate the EPU stress intensity factor for the bounding vertical support plate indication using the results of the CLTP flaw evaluation and a load scaling factor to account for the increase in FIV loading resulting from EPU steam flow.
2. Review the trend of EPU ΔK_{IEQ} to identify if the bounding vertical support indication is predicted to experience further FCG.

The range of EPU FIV ΔK_{IEQ} is calculated by scaling the CLTP ΔK_{IEQ} calculated from finite element fracture mechanics analyses using an EPU FIV scaling factor provided by CDI [4].

The range of EPU FIV K_{IEQ} results are compared against ΔK_{ITH} data to determine if the bounding outer hood vertical support indication is predicted to experience further FCG at EPU operating conditions.

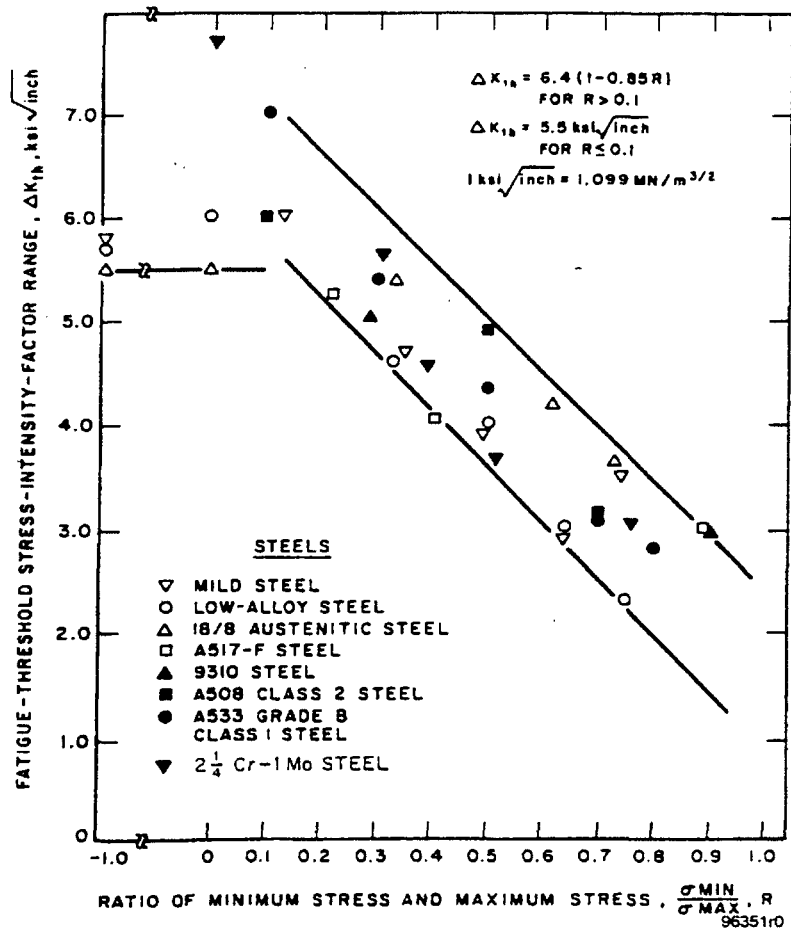


Figure 3-1. Fatigue Threshold Stress Intensity Factor Data [8].

4.0 ASSUMPTIONS

The following assumptions are used for the flaw evaluation:

- The nature of the applied FIV loads acting on the vertical support plate can be treated as displacement controlled loads. This assumption does not suggest that the fluctuating pressure loads are displacement controlled; rather, considering the multiple and redundant load paths existing in the steam dryer structure an increase in local compliance, caused by cracking, in one part of the structure will cause a greater portion of the load to be supported by a parallel load path which results in a reduction in load on the cracked member and a relatively constant displacement on the cracked member. This is a quasi-displacement controlled load.
- System thermal cycles, seismic and hydraulic loads contribute an insignificant number of cycles during the next operating period; therefore, they make a negligible contribution to FCG compared to FIV loading and are not considered here.
- The equivalent stress intensity factor, K_{IEQ} , is expected to be small because the FIV stresses are low; therefore, a plastic zone size correction will also be small and will have an insignificant effect on the K_{IEQ} . Consequently, a plastic zone size correction is not considered in the LEFM analysis.
- The range of alternating stress intensity factor used for calculation of FCG, ΔK_I , is calculated using the range of alternating stress contributed by the FIV loading only. These are the only high cycle fluctuating loads that have the potential to contribute to a significant amount of FCG during an operating period; therefore, these are the only fluctuating loads considered for FCG.
- The distribution of stress range and cycles obtained from the stress time history extracted from the peak stress location of the bounding vertical support plate location in the steam dryer shell model are representative of the range of FIV load and cycle count acting on the vertical support plate. The extent of the sub model is small; therefore, the forced response of the sub model at the peak stress location will have

the same relative amplitudes within a time sample and exhibit the same oscillations as the adjacent region of the sub model.

- The material is assumed to follow linear-elastic isotropic material behavior.

5.0 INPUT DATA

The following data are used as inputs to this evaluation:

- Vertical support plate geometry [6a, 6b, 6c]. The geometry of the outer hood, vertical support plate, cover plate, spacer plate, weld lengths and sizes are provided and verified by CDI [4].
- Indication location, orientation, and size [1].
- The appropriate boundary conditions for the 0-peak CLTP FIV load case model are provided by CDI [4].
- A FIV load case scaling factor to determine EPU loads from CLTP FIV loads equal to {{ }} is provided by CDI [4].
- Sample stress time history at peak stress location in vertical support plate from 3-D shell model is provided by CDI [4].

5.1 Vertical Support Plate Geometry

The INF [1] shows that twelve (12) of the sixteen (16) vertical support plates have reportable indications. There are six (6) vane banks in the NMP2 steam dryer; each bank is reinforced with vertical support plates between the vane assembly and the adjacent hood plate. The vane banks are identified, as shown in Figure 5-1, as the A, B, C, D, E, and F banks. The vertical support plates are fabricated from ¼ inch thick stainless steel plate [6a] which is welded to the vane assembly and hood plates. The weld joint at the vane assembly is defined as a double fillet weld [6c]. For the inner banks (B, C, D, E) the weld joint at the hood is identified as a 0.12 inch square groove weld along the length of the support plate to hood joint [6b]; however, no minimum separation between the hood plates is defined. For the outer banks (A, F), the weld joint at the hoods is identified as a V groove weld with a minimum hood plate spacing of 0.22 inches and a note stating that the weld must tie into the hood support plate [6b]. The outer bank joint design contains an intermediate plate welded between the hoods and the vertical support plate [6b]. For the inner banks, the inspection data shows a double sided fillet weld between the vertical support plate and hoods which appears to extend up the length of the joint for

approximately 4-6 inches [1]. For the outer banks (A, F), the inspection data shows a double sided weld between the vertical support plate and an intermediate plate or spacer plate appearing to extend the full length of the plate. The spacer plate is welded to the hoods with a fillet weld that wraps around the bottom of the spacer plate and extends up both sides for approximately 2-3 inches [1]. The length of these additional welds between the hood plates and vertical support plate and hood plates and spacer plate is not called out on the available steam dryer drawings; however, the weld symbols shown in Reference [6c] suggest the fillet welds are sized at 0.18 – 0.25 inches. Also shown in Reference [6b], and confirmed by the inspection data [1], are notches cut into the vertical support plates, for each of the inner banks, in order to make the fabrication weld called out on Reference [6b]. Based upon the notes in the design drawing [6b], the notches would be made in the field as necessary to make the required welds; thus, there are no design dimensions for the notches. Further, there are no as-built dimensions of the notches. Figure 5-2 is a schematic representing the joint designs for both the inner banks and outer banks.

5.2 Indication Location and Orientation

The INF shows indications in the A, B, C, E, and F vane bank vertical support plates [1]. All indications in the inner bank vertical support plates (B, C, E) are located in the weld material joining the vertical support plate to the hood. All indications in the outer bank vertical support plates (A, F) are located in the weld material joining the vertical support plate to the spacer plate between the hood and the vertical support plate. All indications exist in the hood to vertical support plate weld side rather than in the vane to vertical support plate weld side. The INF [1] identifies sizes for selected indications as:

Vertical Support Plate A2: 1.98 inches (outer bank)

Vertical Support Plate E3: 0.58 inches. (inner bank – includes middle and inner hoods)

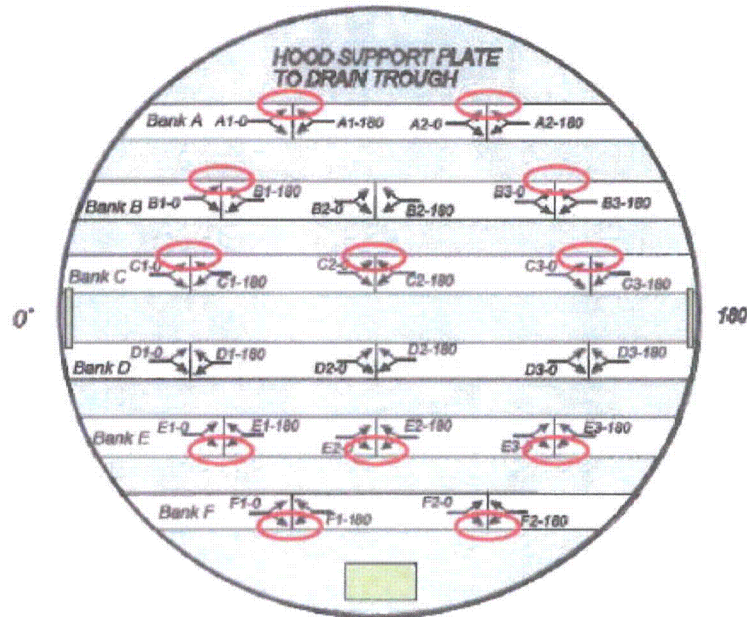
These indications appear to be the bounding crack sizes for the outer and inner banks, respectively. Figure 5-1 identifies the locations of the reported indications [1]. Figure 5-3 contains photographs representative of the indications identified in the INF. The photographs are included in this document to communicate the orientation and size of the indications considered in this flaw evaluation; the INF contains photographs of all indications [1].

5.3 CLTP FIV Loads and Boundary Conditions

The CLTP FIV zero-to-peak steam dryer loads and boundary conditions are obtained from an uncracked steam dryer finite element model (FEM) created by CDI [4]. CDI provided the boundary conditions along with forces and moments applied on all the boundary surfaces of the vertical support plate sub model. Figure 5-4 illustrates the displacement boundary conditions defined by CDI [4]. Figure 5-5 depicts the equivalent applied forces and moments induced by CLTP FIV at each boundary surface provided by CDI [4]. Table 5-1 presents the details of force and moment components applied in each global coordinate direction provided by CDI [4].

5.4 Sample Stress Time History

Sample stress time history data from the 3-D shell model of the NMP2 steam dryer at the peak stress location in the outer hood vertical support plate is provided by CDI [4]. These data are used to determine the cycle counts and relative stress ranges with respect to the maximum stress range of the time record. These statistics are used in the CLTP FCG analysis.



Note: The figure shown above is an excerpt from Reference [1, pg. 2].

Figure 5-1. Schematic Identifying the Location of all Indications in the NMP2 Steam Dryer Vertical Support Plates.

{{

}}

(Note: Displacement A: (0, free, 0); Displacement B: (0, free, free); Displacement C: (0,0,0))

Figure 5-4. Boundary Conditions for the 3-D sub model provided by CDI.

{{

}}

Figure 5-5. Forces (a) and moments (b) Applied on the surfaces of the 3-D sub model.

Table 5-1. Forces and Moments applied on the surfaces.
 (Note: Units are: (lbf) for forces and (lbf in) for moments)

Location	Force, X	Force, Y	Force, Z	Moment, X	Moment, Y	Moment, Z
A. Hood support, positive X	{{ }}	{{ }}	{{ }}	{{ }}	{{ }}	{{ }}
B. Hood support, positive Z	{{ }}	{{ }}	{{ }}	{{ }}	{{ }}	{{ }}
C. Cover plate, negative X	{{ }}	{{ }}	{{ }}	{{ }}	{{ }}	{{ }}
D. Cover plate, negative Y	{{ }}	{{ }}	{{ }}	{{ }}	{{ }}	{{ }}
E. Cover plate, positive Y	{{ }}	{{ }}	{{ }}	{{ }}	{{ }}	{{ }}
F. Hood, positive Z	{{ }}	{{ }}	{{ }}	{{ }}	{{ }}	{{ }}
G. Hood, positive Y	{{ }}	{{ }}	{{ }}	{{ }}	{{ }}	{{ }}
H. Hood, negative Y	{{ }}	{{ }}	{{ }}	{{ }}	{{ }}	{{ }}

6.0 ANALYSIS

This section describes the analyses performed for the flaw evaluation. The following items are discussed separately below:

- Finite Element Model
- Stress Distributions from Uncracked Finite Element Model
- Finite Element Linear Elastic Fracture Mechanics Results
- Stress time history evaluation
- CLTP Fracture Mechanics Evaluation
- EPU Fracture Mechanics Evaluation

6.1 Finite Element Model

Both the uncracked and cracked FEMs are described below.

6.1.1 *Un-cracked Model*

The base FEM used in this evaluation is developed from the 3-D sub model provided by CDI [4]. Figure 6-1 illustrates the configuration of the 3-D sub model of the outer hood vertical support plate configuration. The model is constructed using ANSYS 3-D SOLID45 linear elements. Figure 6-2 shows the mesh defined for this analysis.

6.1.2 *Cracked Models*

For this evaluation, flaws are postulated based on the indications reported in Reference [1]. Two postulated cracks are modeled, one in each fillet weld on either side of the vertical support plate. Each crack front is oriented from the root of the weld to the midpoint of the weld throat surface. In order to evaluate the variation of stress intensity factor with flaw length, six different crack

lengths are modeled. All cracks are modeled as cracks of equal length in both fillet welds. The assumed crack lengths considered are: 0.5", 1.0", 1.5", 2.0", 2.5" and 3.0".

The crack tip for each crack is modeled using the ANSYS 3-D 20-node structural solid element, SOLID95, where the mid-side nodes around the crack tip are shifted to the quarter point locations to capture the singularity in the stress and displacement field near the crack tips. The rest of the FEM is meshed using the ANSYS 3-D 8-node structural solid element, SOLID45. Figures 6-3 through 6-8 illustrate each cracked model created for this analysis.

6.1.3 Boundary Conditions

Figures 5-4 and 5-5 illustrate the displacement and force and moment boundary conditions provided by CDI [4]. The above boundary conditions are first applied to the uncracked FEM developed in this study (referred to force FEM herein). The forces and moments are applied to the surfaces A through H by making use of a pilot node to transfer the loading on the surface. The TARGE170 target element type from the ANSYS element library is used to create the pilot node. The CONTA174 contact element type is used to create a contact surface at the surfaces A through H shown in Figure 5-5. The pilot node and surface are bonded together, so that the forces and moments applied to the pilot node are transferred to the surfaces A through H. Figure 6-9 shows the boundary conditions applied on the uncracked FEM developed in this study.

As assumed in Section 4.0, the nature of the applied FIV loads act on the vertical support plate can be treated as a displacement controlled load. Thus, displacements which create a stress state equivalent to that determined from the force and moment boundary conditions on the uncracked model are applied on the surfaces A through H for all cracked FEMs developed in this study. The displacements were obtained by mapping the nodal displacements on the surfaces A through H obtained from finite element analysis of the force FEM to each cracked FEM. To demonstrate the equivalence between the prescribed displacements and forces and moments on the cutting surfaces, the obtained equivalent displacements have also been applied to the uncracked FEM developed in this study (referred to as displacement FEM herein) on the surfaces A through H.

Figure 6-10 shows the boundary conditions applied on the uncracked FEM with prescribed displacements only.

6.2 Uncracked Stress Distributions

Figures 6-11 and 6-12 show the stress distributions obtained from the uncracked FEMs using both the CLTP FIV force and moment boundary conditions and the equivalent displacement boundary conditions. These figures demonstrate that the equivalent displacement boundary conditions create a stress distribution in the sub model equivalent to the force and moment boundary conditions. Both contour plots also show that the peak stress location is in the vicinity of the observed cracking.

6.3 Finite Element Fracture Mechanics Analysis Results

Figure 6-13 displays the distribution of K_{IEQ} along the crack front for both cracks modeled on either side of the vertical support plate for the 2.0 inch crack case. Results for each crack are referred to as the left and right side cracks. The left side crack refers to the crack shown on the left side of the vertical support plate as seen from the figures of the FEM provided in this section. The right side crack refers to the crack on the other side of the vertical support plate. The results of Figure 6-13 are illustrative of the trend between K_{IEQ} for the left and right side cracks for all of the crack lengths considered. The left side crack is the bounding crack location. It should be noted that the FIV loads are periodic; therefore, it is likely that for the reverse cycle the K_{IEQ} distribution shown in Figure 6-13 would be reversed. The left side crack results are representative of the bounding K_{IEQ} for both cracks and for the full FIV stress cycle.

As shown in the Figure 6-13, the K values on the left and right side cracks have very different values due to the unsymmetrical loads about the support plate. To demonstrate that sufficient elements were used for the cracked FEMs, especially near the crack tip regions, a finer meshed FEM was also developed in this study for the 2.0 inch crack case. Figure 6-14 displays the refined FEM.

H-method mesh refinement was used with a refining factor of 2 along the crack fronts. Compared with FEM shown in Figure 6-6, which contains 36,335 solid elements, the FEM

shown in Figure 6-14 contains 284,896 solid elements. A comparison of equivalent K values between the results of the refined model with that shown in Figure 6-6 was performed and is presented in Figure 6-13. As indicated, there is no appreciable difference in either the trend of K or the values of K on both sides of cracks. The averaged K values for the left side crack are 1.612 ksi-in^{0.5} and 1.644 ksi-in^{0.5} from the respective FEM predictions. The averaged K values for the right side crack are 0.740 ksi-in^{0.5} and 0.766 ksi-in^{0.5} from the respective FEM predictions. Therefore, the FEMs shown in Figure 6.3 through 6-8 are considered acceptable to obtain accurate K values.

Figures 6-15 and 6-16 present the distribution of ΔK_{IEQ} across the crack face for the bounding crack side (Left side) for all crack depths evaluated at CLTP and EPU, respectively. These results are multiplied by a factor of two (2) to convert the K_{IEQ} calculated for the 0-peak FIV loads to a peak-to-peak condition. The EPU results also include a scale factor of 1.382 to account for EPU operating conditions.

Figure 6-17 presents the mean ΔK_{IEQ} calculated for the left side crack at each crack depth evaluated and considering both CLTP and EPU FIV loads. Also shown on this figure, for reference are the dimension of the bounding vertical support plate flaw and the range of ΔK_{ITH} for austenitic stainless steel in air. The ΔK_{ITH} used for this analysis is the lower bound ΔK_{ITH} for a R-ratio of ~0.9; this value is extrapolated from the 18-8 austenitic stainless steel test data presented in Figure 3-1 [8].

Figure 6-18 compares the results of fracture mechanics calculations which explore the effect of load control on the fracture mechanics analysis. As expected, if the applied loading was effectively load controlled then the applied stress intensity factors would continue to increase as the crack grew. These results are discussed in Section 6.5 below in more detail.

6.4 Stress Time History Evaluation

Figure 6-19 displays approximately 120 seconds of the stress time history calculated from the 3-D shell FEM of the NMP2 steam dryer considering CLTP operating conditions [4]. This time history is considered to be representative of the numbers of cycles and relative ranges of stress cycles experienced by the entire sub model. This is not to say that the shell model stress time history is representative of the sub model stress distribution but rather that the number of cycles experienced at this location is representative of the numbers of cycles at all locations in the sub model and that the relative range of stress cycles observed in this time history data is representative of the relative range of stress cycles observed at all locations in the sub model.

The time history data shown in Figure 6-19 is sorted such that all peaks and valleys in the time history record are identified. All points which are not identified as peaks or valleys are discarded from the record. Figure 6-20 and Table 6-1 are a histogram of the time history peaks and valleys. This histogram depicts the counts and cumulative probability distribution of the stress time history. The data analysis was performed using the Excel data analysis add-in.

Conservative stress ranges are determined from the stress time history data summarized in Figure 6-19. The stress ranges are determined from paring peaks and valleys from Table 6-1 such that all peaks and valleys are used. A stress range is determined by representing all counts as the minimum stress from the stress range bin for valleys and the maximum stress from the stress range bin for peaks. Figure 6-21 and Table 6-2 summarize the results of this stress range determination. Table 6-2 also presents scaling factors for each stress range category determined by calculating the ratio between each stress range and the maximum stress range given in Table 6-2. These scaling factors are used with the results of the finite element LEM results presented in Section 6.3 to determine a ΔK_{IEQ} corresponding to each block of stress cycles anticipated for each 120 second FIV time history load at CLTP or EPU operating conditions.

6.5 CLTP FIV Fracture Mechanics Evaluation

Observation of the as-found cracking in 11 of 16 vertical support plates in the vicinity of the peak stress location in the vertical support plate, which all have stopped propagating, combined with the fact that there was no significant change in plant operation in the operating cycle immediately prior to the 2010 refueling outage suggests the following:

1. The cracks initiated shortly after initial plant startup (during the first operating cycle)
2. The loading is displacement controlled

The hypothesis that the cracks initiated shortly after the plant first came on-line is supported by the fact that the plant has experienced no recent change in operating conditions which would cause an increase in FIV loading; therefore, there is no evidence to suggest the cracks are new.

The hypothesis that the applied loading is displacement controlled is supported by the observation that the cracks appear to have arrested. Considering this geometry and loading, if the applied loads were load controlled then the crack driving force would not diminish as the crack grew and the crack would be expected to grow to a significant dimension and result in potential separation of the vertical support plate; fracture mechanics results for this load controlled scenario are presented in Figure 6-18. Conversely, if the applied loading is displacement controlled, then the crack driving force would diminish as the local compliance increased with crack length. This decrease in crack driving force (applied load) would result in a reduction in applied stress intensity factor and eventual arrest of the crack as the applied stress intensity factor decreased below the threshold stress intensity factor for fatigue crack growth.

Figure 6-22 presents the results of a FCG calculation of the bounding flaw in the NMP2 steam dryer outer hood vertical support plate considering the CLTP FIV loads provided by CDI [4]. The analysis is performed to determine if the CLTP FIV stresses result in crack growth and subsequent arrest, consistent with the as-found dimensions of the outer hood vertical support indications identified during the 2010 IVVI [1]. The FCG analysis is performed by scaling the peak to peak CLTP ΔK_{IEQ} results obtained from the sub model using the scaling factors

presented in Table 6-2 and calculating incremental FCG contributed by each block of stress cycles corresponding to the histogram bins presented in Figure 6-21 and Table 6-2.

The results presented in Figure 6-22 suggest that the crack would grow quickly and reach the observed length of approximately 2.0" within a few months of operation. The applied stress intensity factor range is observed to decrease below the threshold stress intensity factor range (ΔK_{ITH}) for FCG of $3.0 \text{ ksi-in}^{0.5}$ which explains the observation of apparent crack arrest.

Considering the local constraint contributed by the spacer plate, fillet welds, and vertical support plate it is assumed that there are relatively large weld residual stresses in the region of the observed crack. The assumed weld residual stresses combined with the deadweight, mean pressure, and steady state thermal loads are expected to result in a R ratio near 0.75-1.0. Review of the experimental data presented in Figure 3-1 support a $\Delta K_{ITH} = 3.0 \text{ ksi-in}^{0.5}$ for a R-ratio in this range. This condition would also make it plausible for a small crack to initiate at the root of the fillet welds by ductile tearing resulting from large weld residual stresses. Once the crack initiated then the FIV loading is shown to be capable of growing the crack to the observed dimension.

Figure 6-17 presents the results of the ΔK_{IEQ} obtained from each of the six crack sizes evaluated considering CLTP conditions. Also shown on this figure is the range of ΔK_{ITH} presented in Figure 3-1 as well as the dimension of the bounding vertical support plate indication. These results show that a crack in the vertical support plate would be expected to grow to approximately 2.0-2.25 inches at CLTP conditions before the crack would arrest because the $\Delta K_I < \Delta K_{ITH}$. These results agree very well with the bounding as-found crack length in the vertical support plate.

6.6 EPU FIV Fracture Mechanics Evaluation

Figure 6-17 presents the results of the ΔK_{IEQ} obtained from each of the six crack sizes evaluated considering EPU conditions. Assuming a lower bound ΔK_{ITH} of $3.0 \text{ ksi-in}^{0.5}$, the results show that a crack in the vertical support plate would be expected to grow to approximately 3.0 inches at EPU conditions. Considering that the local constraint offered by the spacer plate would be expected to diminish above the region of the spacer plate, the weld residual stresses above the

spacer plate would be expected to diminish. This qualitative assessment suggests that the R-ratio above the spacer plate would start to diminish which could result in a higher ΔK_{ITH} as shown in Figure 3-1. Considering a range of ΔK_{ITH} from the lower bound value of 3.0 ksi-in^{0.5} to the upper bound value of 5.5 ksi-in^{0.5}, as shown in Figure 6-17, shows that a crack in the vertical support plate initiated and grown at CLTP would be expected to exhibit a small amount of additional growth ranging from a best case scenario of no additional growth to a worst case scenario of approximately 0.75 inches of additional growth. All values of ΔK_{ITH} suggest that a vertical support plate crack would arrest at a crack length of approximately 3 inches or less.

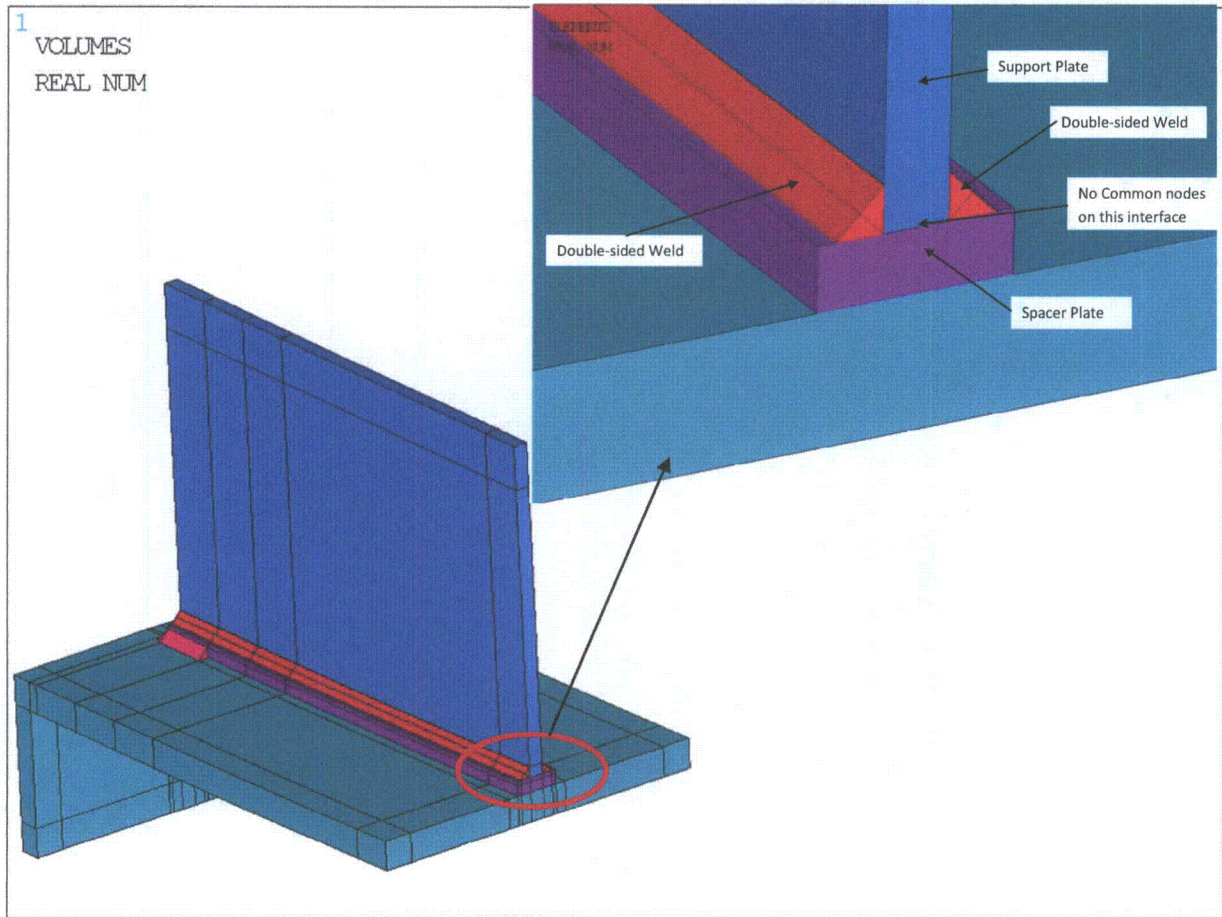


Figure 6-1. Illustration of Double-sided welds between Support and Spacer Plates, outer hood.

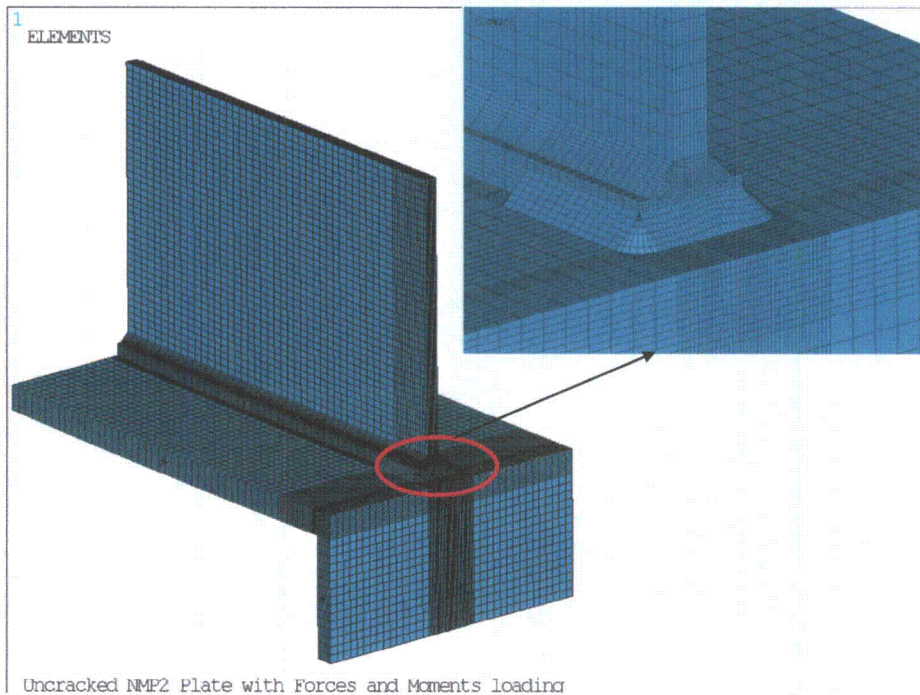


Figure 6-2. Finite Element Model for Uncracked Support Plate Assembly.

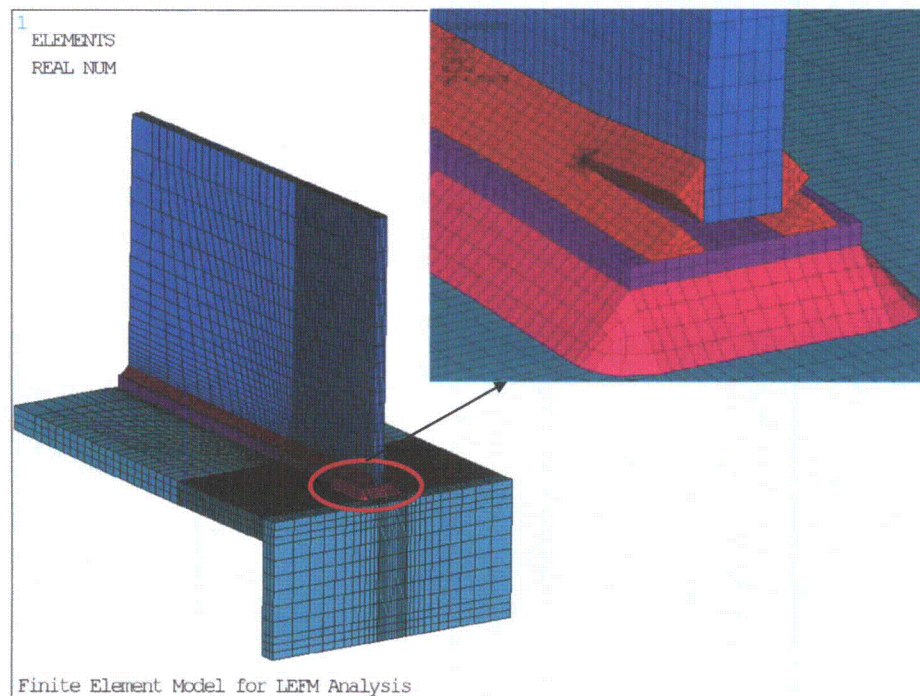


Figure 6-3. Finite Element Model with 0.5" long Double-sided Cracks.
(Note: The cracks were intentionally opened to have better illustration)

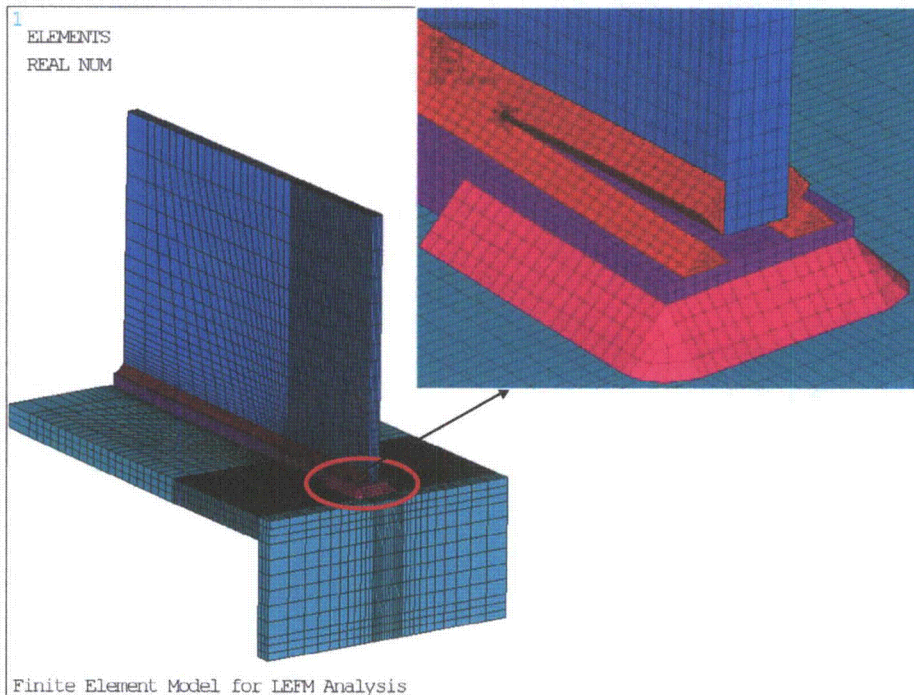


Figure 6-4. Finite Element Model with 1.0" long Double-sided Cracks.
(Note: The cracks were intentionally opened to have better illustration)

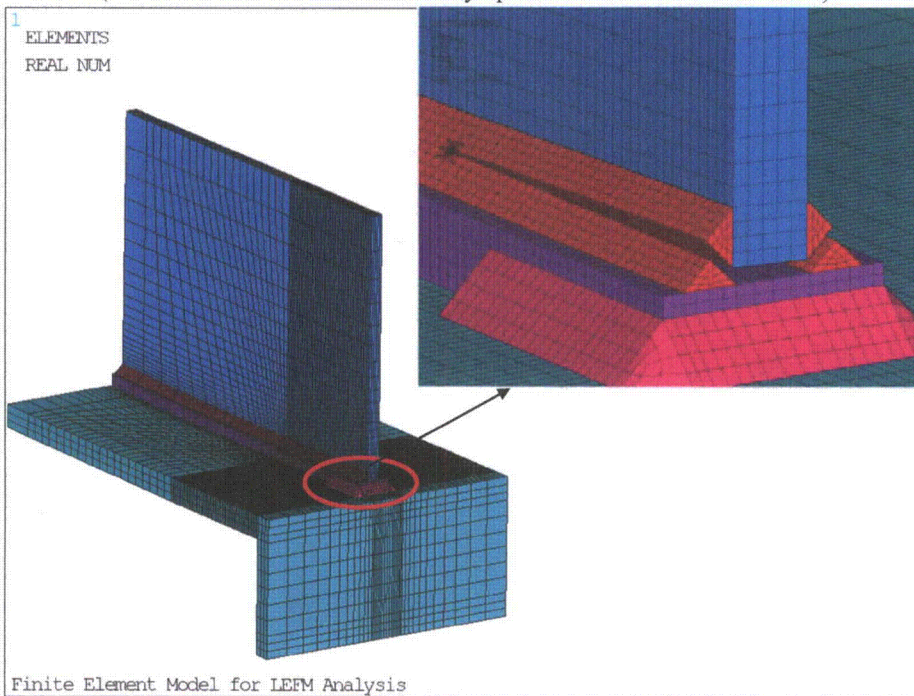


Figure 6-5. Finite Element Model with 1.5" long Double-sided Cracks.
(Note: The cracks were intentionally opened to have better illustration)

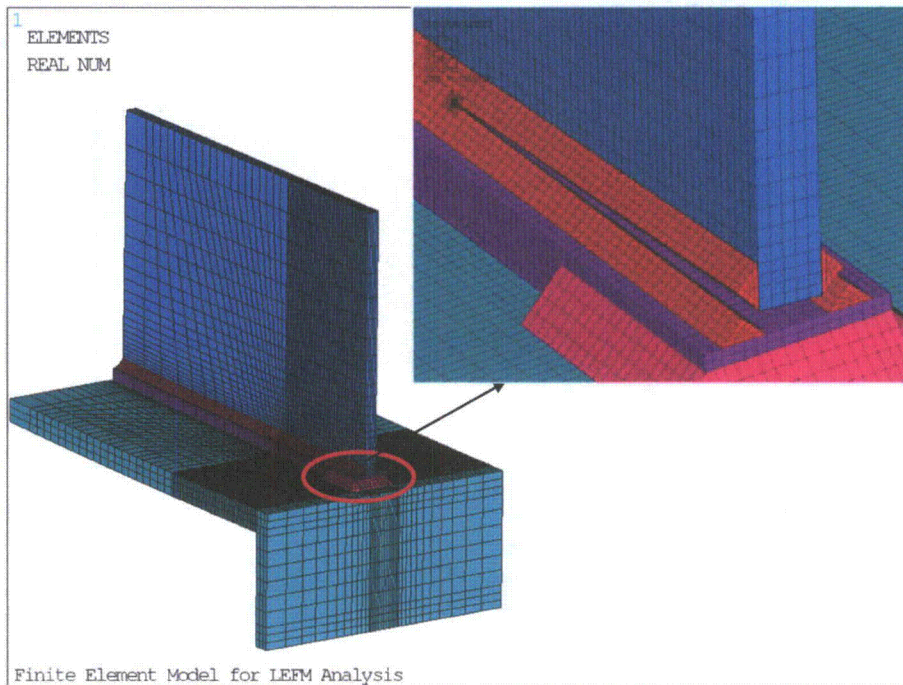


Figure 6-6. Finite Element Model with 2.0" long Double-sided Cracks.
(Note: The cracks were intentionally opened to have better illustration)

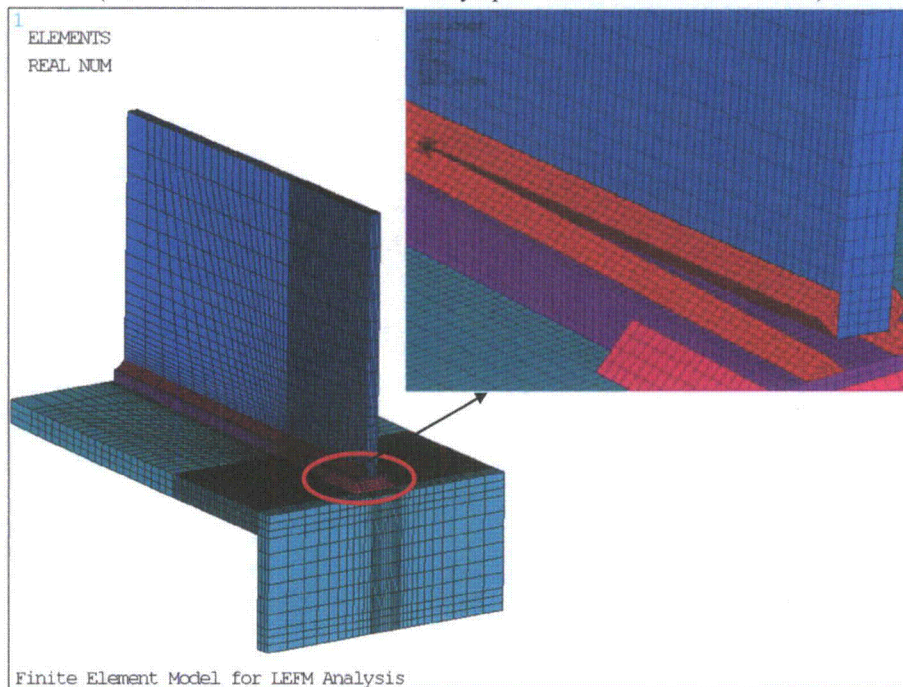


Figure 6-7. Finite Element Model with 2.5" long Double-sided Cracks.
(Note: The cracks were intentionally opened to have better illustration)

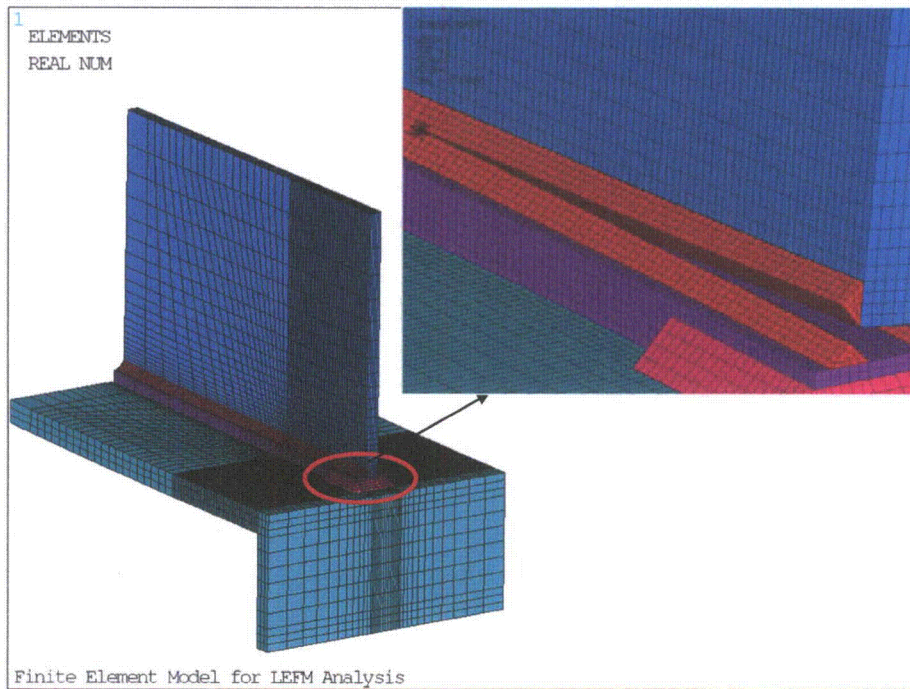


Figure 6-8. Finite Element Model with 3.0" long Double-sided Cracks.
(Note: The cracks were intentionally opened to have better illustration)

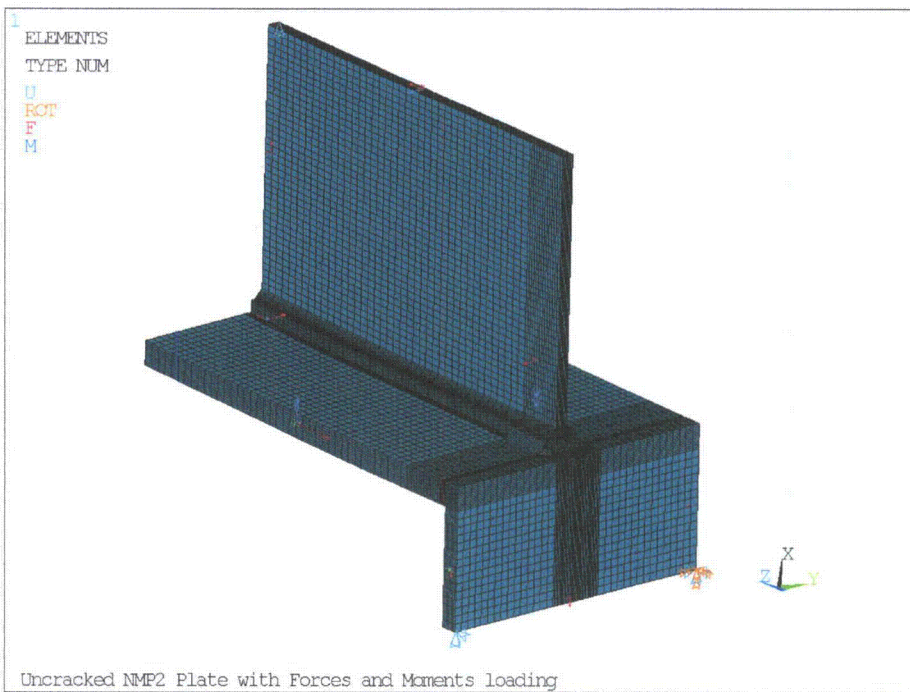


Figure 6-9. Boundary Conditions for the Force FEM.

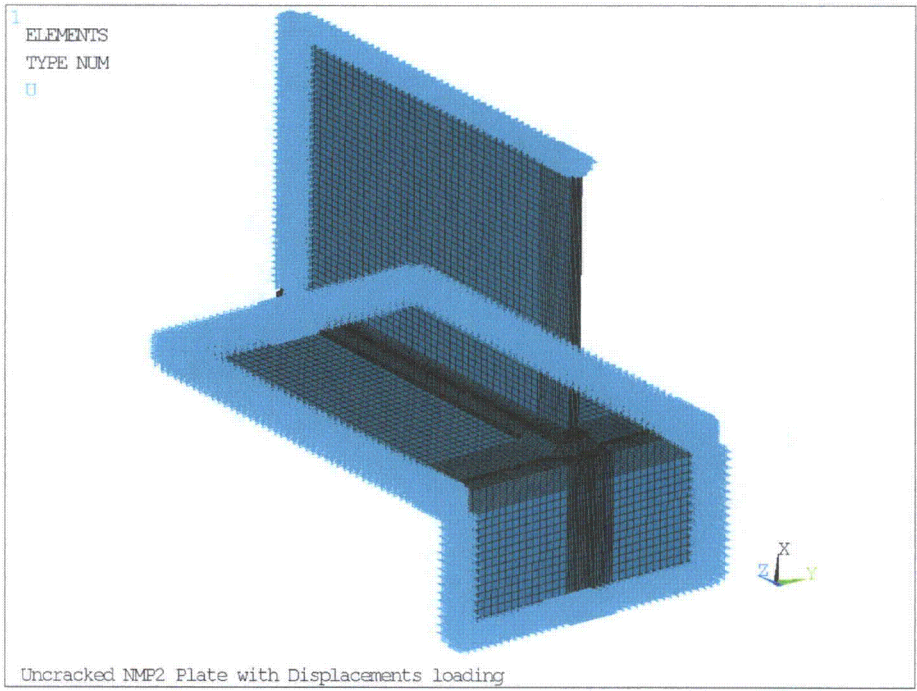


Figure 6-10. Boundary Conditions for the Displacement FEM.

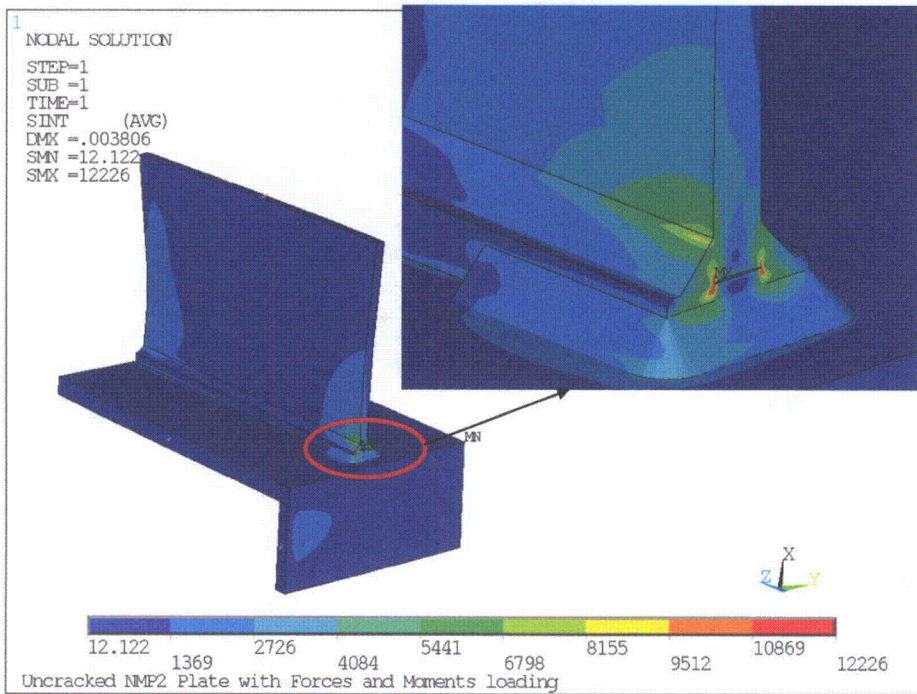


Figure 6-11. Stress Intensity Contours from the Force FEM.

(Note: Units are in psi)

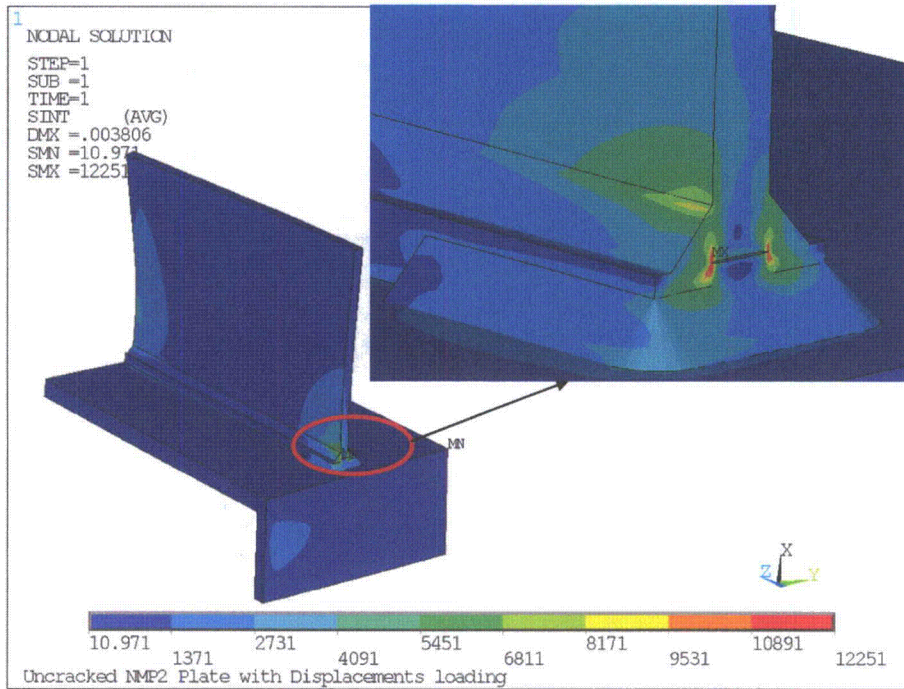


Figure 6-12. Stress Intensity Contours from the Displacement FEM.

(Note: Units are in psi)

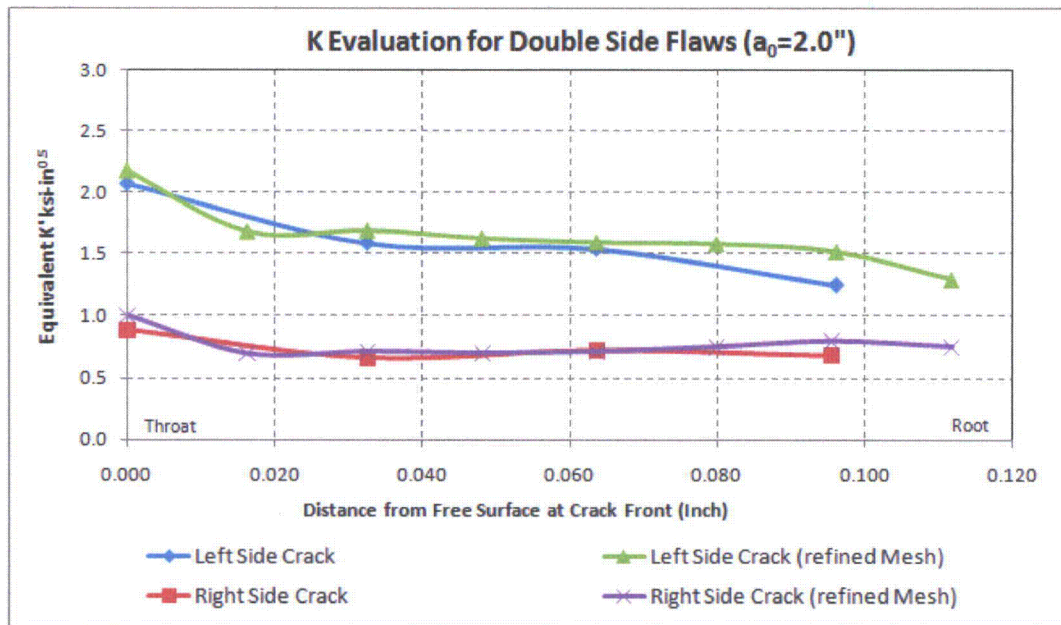


Figure 6-13. K_{IEQ} Distribution along crack front for 2.0 inch Crack Case.

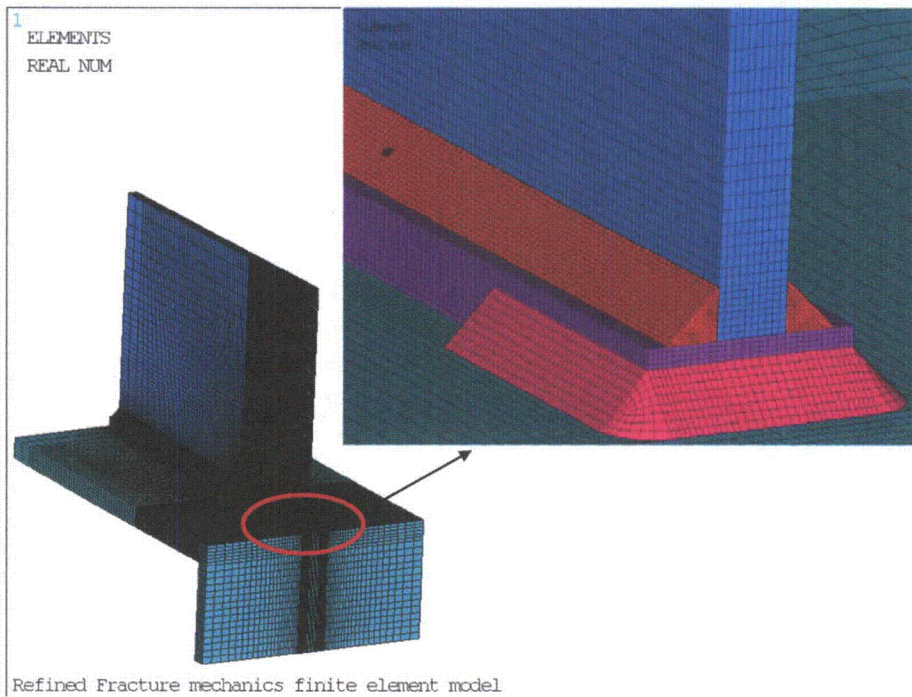


Figure 6-14. Refined Finite Element Model with 2.0" long Double-sided Cracks.

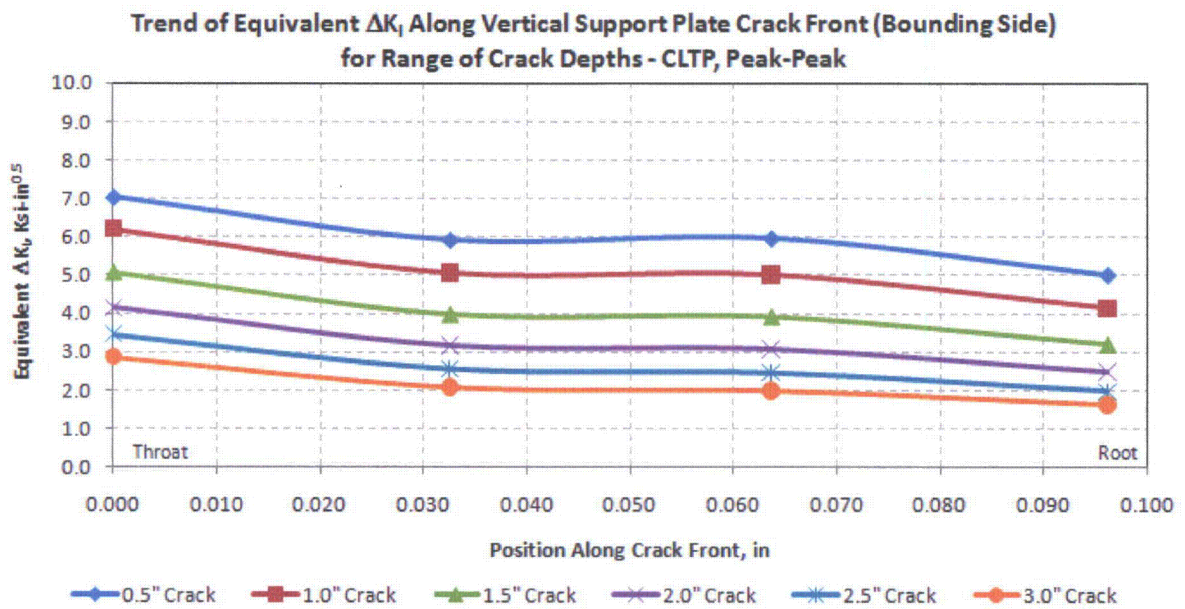


Figure 6-15. ΔK_{IEQ} Distribution across Left Side Crack Front for Various Crack Depths - CLTP.

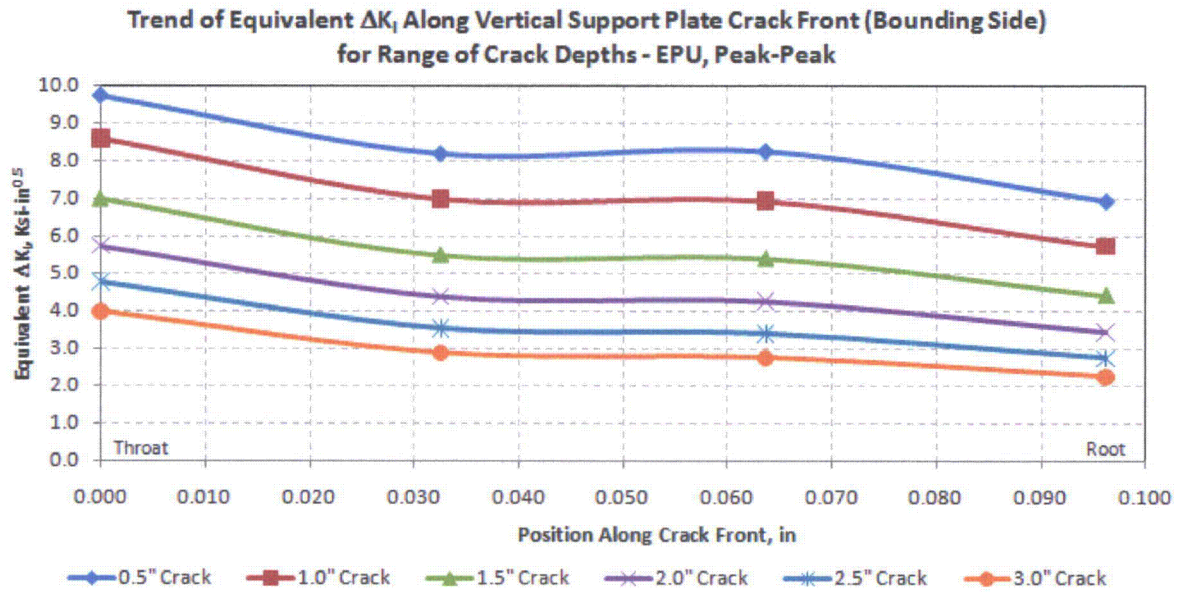


Figure 6-16. ΔK_{IEQ} Distribution across Left Side Crack Front for Various Crack Depths - EPU.

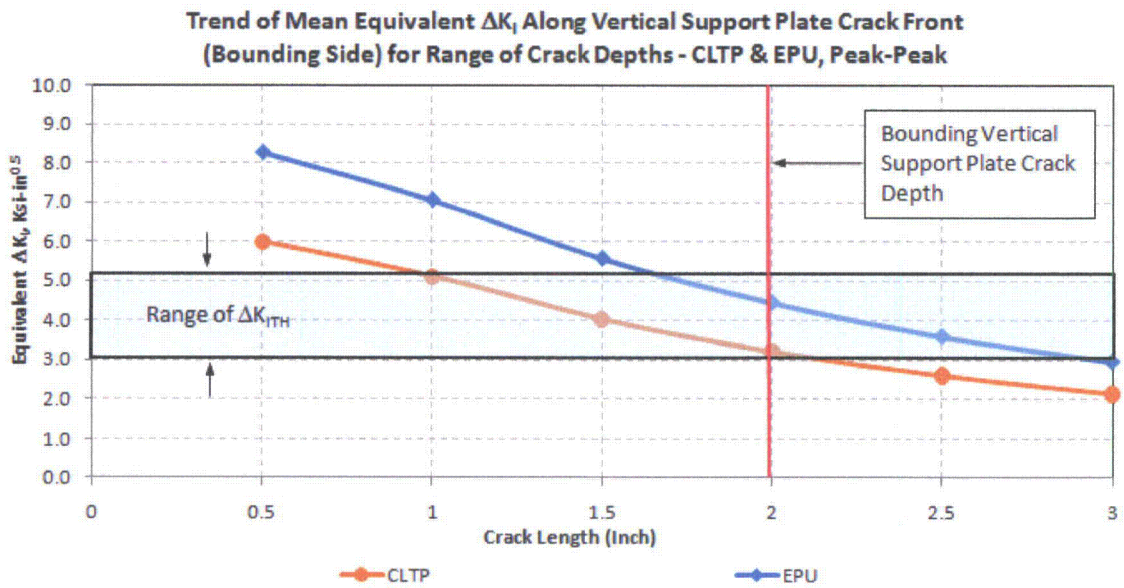


Figure 6-17. Mean ΔK_{IEQ} for Bounding Crack Side (Left Side) for Various Crack Depths.

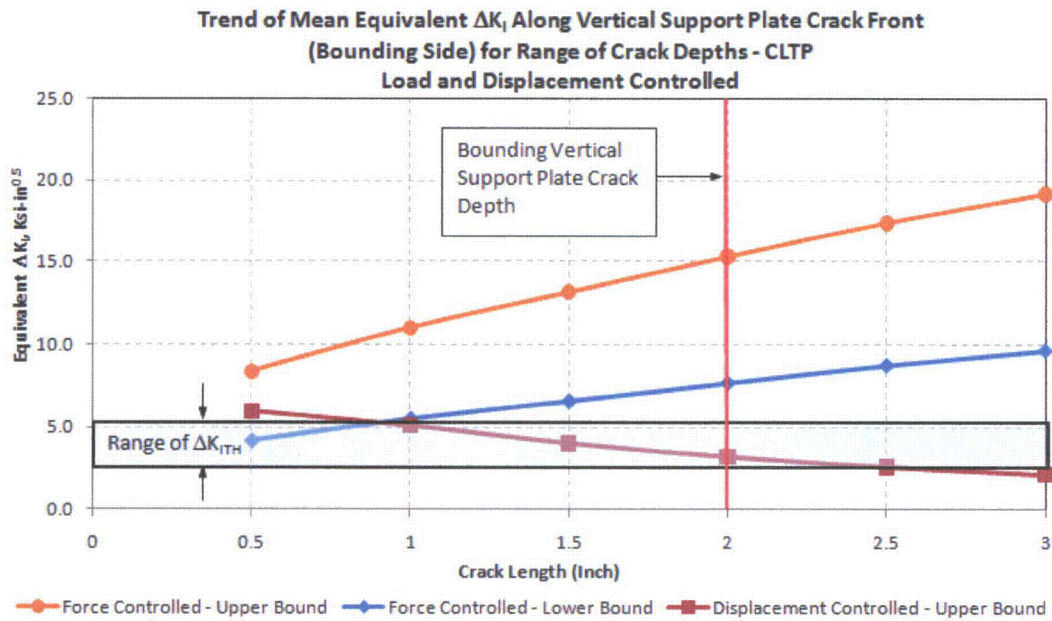


Figure 6-18. Mean ΔK_{IEQ} for Bounding Crack Side (Left Side) for Various Crack Depths, CLTP, Load and Displacement Controlled.

{{

}}

Figure 6-19. 120 Second Stress Time History from Peak Stress Location in Vertical Support [4] Plate – Shell Model, CLTP.

Table 6-1. Stress Intensity Histogram for 120 Second Stress Time History - CLTP.

{{

}}

Figure 6-20. Stress Histogram for 120 Second Stress Time History.

Table 6-2. Stress Intensity Range Histogram for 120 Second Stress Time History - CLTP.

{{

}}

Figure 6-21. Stress Range Histogram for 120 Second Stress Time History.

Outer Hood Vertical Support Plate CLTP Crack Growth Estimate

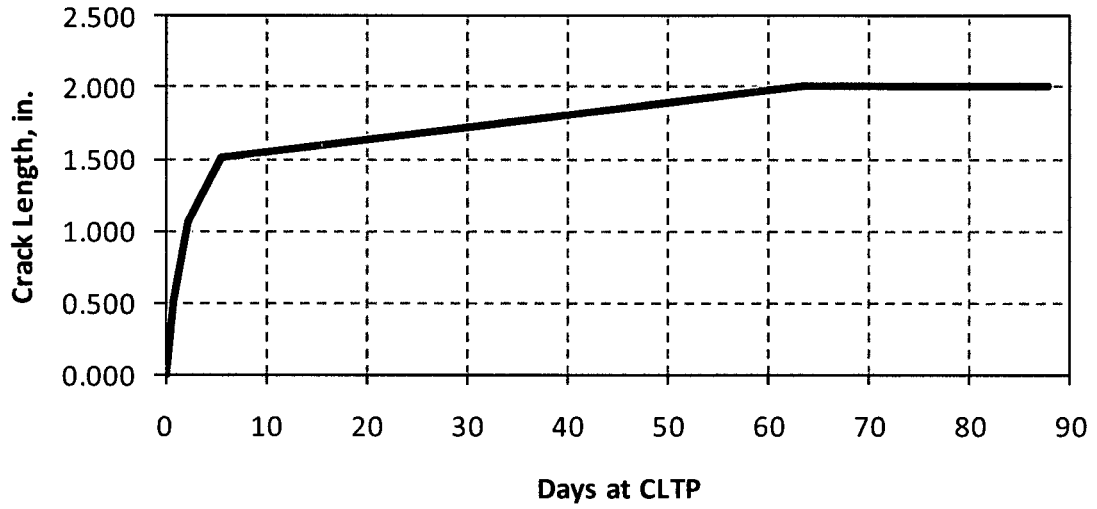


Figure 6-22. Fatigue Crack Growth Calculation for Bounding Vertical Support Plate Indication - CLTP.

7.0 CONCLUSIONS

The results of this evaluation support the following conclusions:

1. A crack initiated at the outer hood vertical support plate would be expected to grow to a length of approximately 2-2.25 inches before arresting at CLTP.
2. A crack initiated at the outer hood vertical support plate at CLTP conditions would be expected to grow to a length of approximately 2-3 inches at EPU operating conditions before arresting.
3. The additional growth experienced at EPU conditions would occur in the first few months of the first operating period at EPU.
4. The middle and inner hoods are bounded by the results of this evaluation.

8.0 REFERENCES

1. Westinghouse Indication Notification Form, "NMP2-RFO-12-INF-10-20-R1", SI File No. 1000506.203.
2. Sommerville, Daniel, "Flaw Evaluation and Vibration Assessment of the Nine Mile Point 2 Steam Dryer for Extended Power Uprate Operating Conditions," Structural Integrity Associates, SI Report No. 0801273.401, Rev. 1, March 2009.
3. Sommerville, Daniel, "Response to NRC RAI Regarding Nine Mile Point Unit 2 Steam Dryer EPU Stress Analysis," Structural Integrity Associates, SI Report No. 0801273.402, Rev. 0, May 2010.
4. Design Input Request for 1000814, Rev.0, SI File No. 1000814.201. **CDI Proprietary Information.**
5. BWRVIP139: BWR Vessel and Internals Project, Steam Dryer Inspection and Flaw Evaluation Guidelines, EPRI, Palo Alto, CA, 2005. 1011463. **EPRI Proprietary Information.**
6. Steam Dryer Drawings:
 - a. GE Drawing No. 158B8534, Rev. 1, "Hood Support," SI File No. 1000506.205.
 - b. GE Drawing No. 795E258, Rev. 0, "Dryer Half," SI File No. 1000506.205.
 - c. GE Drawing No. 795E260, Rev. 0, "Dryer Bank," SI File No. 1000506.205.
7. American Society of Mechanical Engineers, Boiler and Pressure Vessel Code, Section XI, Appendix C, 2001 Edition with Addenda through 2003.
8. J. M. Barsom and S. T. Rolfe, Fracture and Fatigue Control in Structures – Applications of Fracture Mechanics, Prentice-Hall, Inc., 2nd Edition, 1987.
9. ANSYS Mechanical and PrepPost, Release 11.0 (w/ Service Pack 1), ANSYS Inc., August 2007.
10. Anderson, T. L., "Fracture Mechanics Fundamentals and Applications", 2nd Edition, CRC Press, 1995.
11. CDI Report 10-12P, July 2010, "Design and Stress Evaluation of Nine Mile Point Unit 2 Steam Dryer Modifications for EPU Operation. SI File No. 1000814.205P. **CDI Proprietary Information.**

APPENDIX A
INPUT FILE LISTING

The following supporting files are used for this analysis:

Filename	Description
Plate.anf	Geometry file for 3-D Sub-model
AnTip7.MAC	Macro to create crack tip elements
NMP2_Case1.INP	Input file for uncracked Force FEM
NMP2_Case2.INP	Input file for uncracked Displacement FEM
Maprun.INP	Input file to map the results obtained from Force FEM and apply the prescribed displacements on the Displacement FEM
NMP2_BASE_64BIT.INP	Input file to create base cracked FEM so that FEM with different crack sizes can be generated based on this model
NMP2_BASE_64BIT_F.INP	Input file to create base cracked FEM for all the load control cases so that FEM with different crack sizes can be generated based on this model
FM_NMP2_#INCH.INP.INP	Input file to create fracture mechanics models with different crack size and build crack tip elements around the crack fronts, where # = 0.5, 1.0, 1.5, 2.0,2.5 and 3.0
FM_NMP2_#INCH.INP_F.INP	Input file to create fracture mechanics models for the load control cases with different crack size and build crack tip elements around the crack fronts, where # = 0.5, 1.0, 1.5, 2.0,2.5 and 3.0
FM_NMP2_#INCH_LOAD.INP	Input file to apply the prescribed displacements on the cracked model, where # = 0.5, 1.0, 1.5, 2.0,2.5 and 3.0
FM_NMP2_#INCH_LOAD_F.INP	Input file to apply the forces and moments on the cracked model, where # = 0.5, 1.0, 1.5, 2.0,2.5 and 3.0
Load.inp	Applied forces and moments shown in Table 5-1
FM_NMP2_#INCH_KCALC.INP	Input file to extract K results after analysis, where # = 0.5, 1.0, 1.5, 2.0,2.5 and 3.0
FM_NMP2_#INCH_KCALC.CSV	K result outputs, where # = 0.5, 1.0, 1.5, 2.0,2.5 and 3.0
100814.401r0 (Displacement Control).xls	Excel spreadsheet sorting and plotting K results for displacement control cases
100814.401r0 (Load Control).xls	Excel spreadsheet sorting and plotting K results for load control cases
Time Data Processing.xls	Excel spreadsheet used to perform CLTP FCG calculation and prepare histogram of stress time history data